AIAA-2002-2865

Structure of a Supersonic Impinging Rectangular Jet via Real-Time Optical Diagnostics

B. Thurow, M. Samimy and W. Lempert

The Ohio State University
Department of Mechanical Engineering
Columbus, OH 43210

32nd AIAA Fluid Dynamics Conference
June 24 -26, 2002
St. Louis, Missouri

Structure of a Supersonic Impinging Rectangular Jet via Real-Time Optical Diagnostics

Brian Thurow*, Mo Samimy† and Walter Lempert‡
Gas Dynamics and Turbulence Laboratory
The Ohio State University
Columbus, OH 43210

A real-time imaging system is used to investigate the flow field of an impinging Mach 1.3 ideally expanded rectangular jet. Far field acoustic data show a variety of impingement tones. The most dominant tones occur for a Strouhal number (based on nozzle exit height) range between 0.2 and 0.25. Impingement plate locations of ℓ = 70, 105, 115 and 356 mm were further analyzed as they characterize various states of the impingement flow. These locations were also investigated using the real-time flow visualization technique in order to correlate the dynamics of the flow's mixing layer with its acoustic far field. There is a strong coupling between the organization of structures within the flow field and the degree of resonance observed in the acoustic far field. The most resonant case of ℓ = 70 mm exhibited many high amplitude harmonics as well as a very organized asymmetric pattern of large-scale turbulence structures. No impingement tones above 110 dB were observed at ℓ = 105 mm, while a single tone greater than 125 dB was present at ℓ = 115 mm. The flow fields of ℓ = 105 and 115 mm were similar with ℓ = 115 mm containing larger and more developed structures at the flow/plate interaction region.

Introduction

Recently there has been growing interest in the field of aero-optics as laser and imaging systems are being used more frequently in military aircraft. Typical applications include imaging systems, laser radar, laser guided bombs and directed energy systems such as that on the new airborne laser aircraft. The overall success of these systems is ultimately limited by the wavefront degradation that occurs as a light beam traverses the turbulent flow over the observation/transmission window on an aircraft's body. Recent studies (e.g. Truman and Lee, 1990; Chew and Christiansen, 1993; Jumper and Hugo, 1995; Fitzgerald and Jumper, 2002) have focused on numerical simulations and experimental techniques that can produce time-correlated data of the optical wavefront degradation. Currently, however, experimental techniques are limited in their combined temporal and spatial resolution with the trade-offs between the two being quite significant.

Recently at the Gas Dynamics and Turbulence Laboratory (GDTL) of OSU, we have demonstrated a real-time flow visualization technique that can acquire high spatial resolution flow images at a variable rate up to 1 MHz (Thurow et al., 2001 & 2002). Coupled with a MHz rate Shack Hartmann wavefront sensor currently under development, we are developing an experimental technique with the ability to simultaneously measure both the flow field and degraded optical wavefront at sampling rates up to 1 MHz. The main advantage of this new technique is its ability to be used in high-speed compressible flows, which are more representative of the flow encountered in flight. This new technique will offer significant improvement in combined spatial and temporal resolution. In order to develop this new technique, a trial flow field is needed for testing. An ideal flow field would be one whose characteristics are well known and one that renders some control over its main characteristics. One such flow field is a supersonic impinging jet. The goal of this paper is to apply real-time flow visualization to a supersonic impinging jet in preparation for the next step of incorporating a real-time Shack-Hartmann wavefront sensor. Therefore, aero-optics will not be addressed in this paper, but will be addressed in future publications featuring the impinging jet and flow visualization system of this study.

Impinging jets are characterized by a strong coupling between flow and acoustic fields and a self contained feedback mechanism that result in high amplitude sound tones. The feedback mechanism is well studied (e. g. Rockwell and Naudascher, 1979; Ho and Nosseir, 1981; Tam and Ahuja, 1990; Krothapalli et al., 1999; and Alvi et al., 2002) and briefly described here. The feedback loop begins with the formation of turbulence structures within the shear layer of the jet. These structures grow and convect downstream where they interact with the impingement plate. Acoustic waves are created due to this interaction and travel outside of the flow in the upstream direction. These acoustic waves/perturbations eventually reach the receptivity location of the shear layer at the nozzle exit

* Graduate Student, AIAA Member
† Professor, AIAA Associate Fellow; Corresponding author
‡ Associate Professor, AIAA Associate Fellow

where they excite the shear layer and lead to the formation of more structures, thus perpetuating the cycle. Ho and Nosseir (1981) found that the frequencies produced could be predicted quite well by requiring that an integer number of waves, N, exist in the feedback loop according to the equation:

$$N = \frac{f\ell}{U_c} + \frac{f\ell}{a_o} \tag{1}$$

where f is the frequency, ℓ is the distance between the nozzle exit and the impingement plate, U_c is the convective velocity of turbulence structures and a_o is the ambient speed of sound.

While describing the frequency modes fairly well, equation 1 does not provide any information about the flow field, which can be quite complex. The initial formation of turbulence structures within the shear layer is largely dependent on the frequency(ies) of forcing. The development of structures is further influenced by the strong interaction between the flow and the plate. The connection between structures and impingement tones has been studied in the past using techniques such as schlieren imaging (e. g. Krothapalli, 1985; Tam and Norum, 1992) and recently using PIV (Krothapalli et al, 1999; Alvi et al., 2002). Using these techniques researchers have explored different branches of the feedback loop and identified different impingement tones as originating from symmetric or asymmetric modes within the shear layer.

This paper uses the real-time imaging system to investigate in more detail the flow field of an impinging rectangular supersonic jet. In particular, the connection between the acoustic tones and the development of large-scale structures within the mixing layer is explored.

Experimental Facilities and Set-up

Impinging Jet Facility

All of the experiments were conducted at The Ohio State University's Gas Dynamics and Turbulence Laboratory (GDTL). The facility consists of a jet stand and stagnation chamber to which a variety of nozzles may be attached, an anechoic chamber and an impingement plate and stand. Air is supplied to the stagnation chamber from two four-stage compressors; it is filtered, dried and stored in two cylindrical tanks with a total capacity of 42.5 m^3 at 16.5 MPa (1600 ft^3 at 2500 psi). The stagnation chamber contains a perforated plate and two screens of varying porosity to condition the flow to be uniform prior to entering the nozzle.

The nozzle used in this study is a converging-diverging rectangular nozzle with exit dimensions of 38.1 mm width (w) x 12.7 mm height (h) (1.5" x 0.5", aspect ratio of 3) and has a lip thickness of 6.35 mm (0.25"). It attaches to the stagnation chamber via a circular to rectangular adapter. The contour of the nozzle was designed using the method of characteristics for uniform Mach 1.3 flow at the exit; experimentally, the Mach number was determined to be 1.28. Pressure to the stagnation chamber and the nozzle is regulated manually through the actuation of a Fisher control valve and is held constant to within 0.3 psi. For all experiments herein, the pressure was maintained for ideally expanded flow.

The flow from the nozzle exhausts into a fully anechoic chamber. The chamber measures, from wedge tip to wedge tip, 3.12 meters in width and length, and 2.69 meters in height. An open area has been built around the perimeter of the front wall to allow for adequate entrainment of ambient air by the jet with a bellmouth placed on the opposite wall of the chamber for air to exit the chamber. The chamber was tested for compliance to ANSI Standard S12.3535, and the results from the tests were within the required tolerance over most of the distances along the microphone paths (Kerechanin et al. 2000). Further details of this facility can be found in Hileman and Samimy (2001) and Kerechanin et al. (2000).

The impingement plate consists of a 304.8 mm (12") diameter circular aluminum plate with a thickness of 31.75 mm (1.25"). The front edge of the plate is smooth and rounded with a 12.7 mm (0.5") radius of curvature for smooth separation of the flow from plate. The plate is mounted on its back face to a sliding aluminum rail, which in turn is mounted to a stand made out of steel 'L' beams. The stand is bolted to the floor in four places and was constructed to minimize vibrations from the impinging flow. The plate can be moved along the rail to be positioned anywhere from 0 to 356 mm (28 nozzle heights) from the nozzle exit with better than 1 mm accuracy. It should be noted that the impingement plate facility was not designed to simulate a ground environment (i.e. a STOVL type application), but was designed as a means of generating a resonance condition and thus well-organized structures. Future work using this facility will attempt to use flow control actuators to modify the characteristics of the flow with or without the resonance and thus will look into the effects of forcing on the flow with the presence of relatively disorganized and well-organized structures.

Acoustic Measurements

Acoustic data were obtained using a 6.35 mm (quarter inch) microphone (B&K Model 4135) mounted 698.5 mm (27.5") directly above the nozzle centerline and 25.4 mm (1") downstream of the nozzle exit (~ 88° from the jet axis). The microphone was oriented perpendicular to the major axis of the rectangular

nozzle and attached to a vertical rail wrapped in acoustic foam to minimize reflections from its surface. The microphone was connected to a B&K Nexus conditioning amplifier and the signal filtered at 100 kHz. The signal was then sampled at 200 kHz using a National Instruments PC-6110E data acquisition board. Data were obtained for impingement plate separations, ℓ, from 20 mm to 200 mm. In general, sound data were acquired in 5 mm intervals except for between 160 and 200 mm where the interval was 10 mm. Additional measurements were made at 62.5 and 67.5 mm after the initial run to assess the repeatability of the measurements. Data were also obtained with the impingement plate at its furthest location (ℓ = 356 mm) as well as with the plate and stand removed from the chamber. For each data point, data were obtained in 100 blocks of 4196 points each (>2 sec total). Following acquisition, the data were taken to frequency domain using a Matlab based FFT algorithm.

Real-time Flow Visualization Technique

A pulse burst laser and an ultra high-speed CCD camera were used to take sequences of 17 time correlated flow visualization images. The pulse burst laser has been described elsewhere (Lempert et al., 1996, 1997, Wu et al., 2000, Thurow et al., 2001) and only a short description will be provided here. The laser is a custom built 2nd generation Nd:YAG laser system that achieves a high repetition rate through the use of a dual Pockel cell arrangement. The output is frequency doubled at 532 nm (green). The laser is flexible and can create between 1 and 99 pulses over a time span of approximately 150 microseconds and can operate at a maximum rate of 1 MHz. Due to camera limitations the laser was set to generate 17 pulses. In order to use the full time range of the burst of pulses, inter-pulse timing was set to 8 microseconds. Each pulse is 10 nsec in duration and contains an average of 7 mJ per pulse. The overall repetition rate of the system is 10 Hz.

For flow visualization, the laser beam was formed into a sheet and passed through a streamwise plane in the flow. Seed particles were introduced into the mixing layer using natural product formation where water contained in the warm moist ambient air condensed upon entrainment into the jet and mixed with the cold and dry air of the jet core. Concerns about the size of the particles formed and the response time of their formation have been previously addressed, and the particles are believed to accurately mark the major features of the shear layer (Elliott et al., 1992). Laser light scattered from the condensed water particles was then captured and recorded using a Dalsa 64K1M 12-bit CCD camera. This camera can capture 17 images with a resolution of 245 x 245 pixels at a rate up to 1 MHz. Due to the masking technique used to create the high frame rate, the fill factor of the camera is on the order of 3% with an effective pixel size of ~ 10 microns. Despite this limitation of the camera's sensitivity, the combination of the laser and camera is still sufficient to visualize the flow.

Flow visualization was performed with the impingement plate at 4 different locations (ℓ = 70, 105, 115 & 356 mm). These locations were chosen based on the results of acoustic measurements and will be discussed later. In each case the laser sheet was formed in the streamwise direction and directed to illuminate the region of the jet immediately before and up to the impingement plate. The camera was outfitted with an f/# 1.2 50 mm focal length lens and placed perpendicular to the flow approximately 150 mm from the jet. In general, the camera's field of view was approximately 50 to 100 mm square. Fifty image sequences were acquired for each impingement plate location. After acquisition, each image was post-processed using Matlab and saved in movie format for analysis. Post-processing consisted of a background subtraction, a smoothing filter (3 x 3 pixel moving average) and a normalization process to correct for shot-to-shot non-uniformity of the laser sheet intensity.

Experimental Results and Discussion

Acoustic Measurements

Acoustic measurements were made at various nozzle/plate separation distances, ℓ, spanning from 20 to 200 mm (ℓ/h = 1.57 to 15.7). For each location, spectra were created and analyzed for their tonal content. Figure 1 is a summary of all the identified tones with amplitudes over 100 dB. The figure exhibits a very rich content of impingement tones at varying magnitudes and frequencies. Over 20 tones can be identified in some cases (e. g. ℓ = 50 mm) while other cases exhibit a few tones (e. g. ℓ = 105 mm). In general, the frequency of the fundamental tones decreases with increasing separation distances. At certain locations, the well-known staging phenomenon is also apparent. These features are better observed in Figure 2, which only shows the most dominant tones.

Figure 2 is a non-dimensional plot of all tones with magnitude larger than 115 dB. The scaling and staging phenomenon is quite evident and the fundamental tones generally fall in the range of St_h = 0.2 to 0.25. This agrees with the theoretical model of Tam and Ahuja (1990). Naturally, the harmonics are between St_h = 0.4 and 0.5. The figure also includes the impingement frequencies predicted by Equation 1 (Ho and Nosseir, 1981). The convective velocity used for this equation

was not measured experimentally, but set to be $0.59U_j$, as it achieved the best curve fit through the experimental data. This value of convective velocity is within the range of convective velocity used by other researchers (Ho and Nosseir, 1981, Krothapalli, 1985, Raman and Rice, 1994, Krothapalli et al., 1999). Overall, the experimental data are accurately represented by Equation 1 with only some slight disagreement. Most of the observed tones with magnitude under 115 dB and not shown in Figure 2 also are well represented by Equation 1. The slight disagreement between the predicted and measured frequencies may be due to variations of the convective velocity with the separation distance and changes in the ambient temperature. Overall, the observations made here are in good agreement with numerous other studies on impinging jets and fairly well documented in the references given above.

The focus of this work, however, is not strictly on the impingement tones, but, rather, on the flow field that creates and is also affected by these tones. The impingement tones are, therefore, treated as a signature of the flow field and used to identify some interesting cases for flow visualization. In this respect, four plate locations were chosen to characterize various regimes of the impinging jet. The spectra of these four cases will be examined in further detail below followed by presentation of flow visualization results. The first case chosen is the baseline case where the plate is placed a long distance from the nozzle and thus its effect on the flow is expected to be minimal. The second location is where the jet exhibits many strong impingement tones and thus the flow is expected to be strongly influenced by the presence of the plate. The third and fourth cases correspond to a transition from a very weak impingement tone to a very strong one. The spectra of these four locations are examined below. The flow visualizations will be examined in the next section.

Figure 3 is the baseline case and shows spectra of the jet without the impingement plate and with the impingement plate placed at 356 mm (the farthest back it could go). The two spectra are nearly identical in both frequency content and amplitude for frequencies above 7 kHz. Below 7 kHz, the impinging jet has higher amplitude broadband noise content emanating due to the interaction of the impingement plate and the jet. There are no identifiable impingement tones produced in this arrangement, however. The most notable feature of the spectra is the presence of screech tone and its harmonic occurring at 7.4 and 14.8 kHz with amplitude of ~110 dB. Although the jet is ideally expanded, the rectangular geometry leads to the formation of weak shocks and their interactions with flow structures that produce the screech tones. These tones, while significant, do not approach the amplitude of the strongest impingement tones (125+ dB) and are suppressed in the presence of strong impingement tones, as will be discussed later. Therefore, they only appear for separation distances of 150 mm or greater (ℓ/h >11.8), where impingement tones are not present. The presence of screech tones in ideally expanded supersonic jets has also been observed in rectangular jets by Raman (1997).

Figure 4 is a spectrum of the jet when the impingement tones are near their strongest levels. Although many plate locations had strong impingement tones, this plate location of ℓ = 70 mm (ℓ/h = 5.5) was used for flow imaging due to its convenience from an imaging standpoint. The fundamental tone is at 6 kHz (St_h = 0.2) and 128 dB and harmonics can be identified as far out as 66 kHz. There is no evidence of screech tone and the impingement tone is nearly 30 dB above the background. The spectrum of Figure 4 consists of an unmistakable fundamental frequency and its harmonics. The presence of this many harmonics is also evident at many other plate locations. For example, at l=45 mm (ℓ/h = 3.54), harmonics greater than 100 dB can be clearly identified beyond 80 kHz. Other plate locations with strong harmonic content yield spectra with even more tones. In some cases, over 20 discrete tones can be identified. For example, at ℓ = 50 mm (ℓ/h = 3.94), peaks greater than 100 dB were recorded at 2.65, 3.6, 4.25, 4.6, 6.25, 7.84, 9.4, 10.5, 11.4, 12.5, 14.1, 15.7, 18.7, 20.3, 21.9, 23.5, 26.6, 28.2, 29.8 and 43.9 kHz. Unlike in Figure 4, most of these tones do not appear to originate from a single fundamental, but from the two highest amplitude tones of 6.25 kHz and 7.84 kHz. Most of these tones are linear combinations of these two fundamentals (e. g. 9.4 = 2*7.84 – 6.25, 14.1 = 6.25 +7.84, 21.9 = 6.25 + 2 * 7.84, etc.) A similar observation was made by Tam and Norum (1992) on a Mach 1.29 rectangular jet with aspect ratio 4.24.

Although many plate locations were quite rich in harmonic content, some other plate locations yielded very little. Figure 5 is the spectrum at ℓ = 105 mm (ℓ/h = 8.27). Although some peaks (6.5 and 13 kHz) are present, they do not rise much above the background and do not exceed 110 dB. With the plate moved 10 mm downstream, however, to ℓ = 115 mm (ℓ/h = 9.1), a very strong impingement tone appears at 12 kHz with an amplitude of 126 dB. This spectrum is shown in Figure 6. This fundamental tone appears to be at 6 kHz with amplitude of 111 dB. The fact that the harmonic is more intense than the fundamental could be due to the location of the microphone relative to the impingement plate. Outside of the impingement tones, the spectra of Figures 5 and 6 compare well. It is the emergence of the impingement tone with the placement of the plate that is of most interest, however, and this phenomenon

is explored in more detail using flow visualization in the next section.

MHz Rate Flow Visualizations

Flow images are presented for four different plate locations (ℓ = 70, 105, 115 and 356 mm). Each plate location was chosen to represent a unique characteristic of the flow field based on the acoustic measurements. Figure 7 shows the average of 50 images acquired at each location with the jet and impingement plate shown schematically to orient the reader. Flow is from left-to-right and only the mixing layer is visualized due to the product formation seeding technique used in this study. Due to the camera's field of view and limited laser power, the entire flow field was not captured and thus the images may appear cutoff in the upstream side for all four cases and also downstream side for the last case. The effect of the impingement plate on the flow field is obvious as the flow is gradually deflected parallel to the plate. The mixing layer grows very rapidly in the presence of the impingement plate compared to the baseline case, which is similar to the last case, as it is in an excited and organized state. The presence of a compression region marked by a curved front in the flow and the impingement plate interaction region is also evident and roughly the same size for the three impinging cases. Following the deceleration of the flow within the compression region, the flow exits the visualized region in a direction parallel to the plate. More detailed characteristics concerning the dynamics of these four flow fields will be examined below.

Figure 8 is a sequence of 4 (out of 17) images of the baseline flow field and is a typical example of the images obtained. The viewing area extends from 61 mm to 171 mm (~ 4.8h to 13.5h) downstream of the nozzle exit. Each image in the figure is separated by 40 microseconds. The full sequence of images (not shown here due to limitations of the paper format) is comprised of 17 images separated by 8 microseconds each and can be viewed as a movie at http://rclsgi.eng.ohio-state.edu/~samimy/GDTL. These images show a flow field with a wide variety of turbulence scales superimposed on a somewhat organized pattern of large-scale structures. The variety of scales is evident in the jagged edges of the mixing layers on both the high and low-speed sides of the flow. Structures 'A' and 'B' are marked in the first frame of Figure 8 and are typical examples of the types of large-scale structures and with an asymmetric pattern seen in the baseline flow field. These structures undergo, in general, the processes of 'tilting', 'tearing', 'stretching' and 'pairing' that are typically seen in high-speed jets of similar Mach number (Thurow et al., 2001). Structure 'A' exhibits some of these features as it tilts and stretches through the four frames shown in Figure 8. The overall nature of this baseline flow field is quite similar to an earlier study conducted on a Mach 1.3 axisymmetric jet with the same imaging system (Thurow et al., 2001). The rectangular jet is more organized than the axisymmetric jet and *consistently exhibits the asymmetric pattern of structures*. Unlike the axisymmetric jet, however, the jet in this study exhibits a screech mode, which means that there is a strong coupling between the flow and acoustic field that provides self-excitation and may explain the organized pattern observed.

Figure 9 is a sequence of 4 images (out of 17) of the flow field with the impingement plate located 70 mm from the nozzle exit. The viewing area extends from 12 mm to 71 mm (~ 1h to 5.6h) downstream of the nozzle exit. In stark contrast to the baseline flow field, this impinging flow field is very well organized and dominated by fast growing structures arranged in an asymmetric pattern. The structure marked 'A' in frames 2 and 4 is a typical example of this rapid growth. While not apparent in the set of images in Figure 9, the full sequence of 17 images (not shown here) shows the growth of structure 'A' occurring due to a 'roll-up' mechanism. The structures that form are distinctly separate from the rest of the mixing layer and typically interconnected with a braid region similar to that seen in incompressible shear layers. Furthermore, compared to the images of Figure 8, the flow field does not seem to exhibit nearly as many turbulence scales. The structures and events depicted in Figure 9 are extremely repeatable and consistent throughout the entire set of 50 movies taken. The fundamental peak in the spectrum of Figure 4 is at 6 kHz (period = 167 microseconds) and, not surprisingly, structures form, grow while convecting downstream, and 'crash' into the plate at the same rate on each side of the mixing laser. As the large-scale structures on either side of the mixing layer are offset in an asymmetric pattern, they interact with the plate at an overall rate of 12 kHz, which is the strong harmonic tone present in Figure 4. It is quite evident that there is a strong coupling between the organization of the self-excited mixing layer and the impingement tones produced.

Figures 10 and 11 are typical image sequences of the flow field with the impingement plate at 105 and 115 mm, respectively. The images in Figure 10 visualize the jet 44 to 104 mm (~ 3.5h to 7.1h) downstream of the nozzle exit while those in Figure 11 covers 53 to 113 mm (~ 4.2h to 7.7h). Thus, the scale of each image is the same and depicts the region of the jet immediately upstream of the plate. The change of ~0.7h in the location of the impingement plate between these two cases, however, has a profound effect on the flow's acoustic characteristics (see Figures 5 and 6). For ℓ = 105 mm, recall that there are no tones over 110 dB (there are some under 110). At ℓ = 115 mm,

however, there is an impingement tone over 125 dB in magnitude at 12 kHz. Here we attempt to make a correlation between the impingement tones in the acoustic far field and the characteristics of the turbulence structures in the mixing layer.

Upon first glance, Figures 10 and 11 look very similar. Both flows contain larger structures arranged in an asymmetric pattern. The structures are more organized than the baseline flow (Figure 8), but do not exhibit the same degree of organization as the highly resonant case of ℓ = 70 mm (Figure 9). Despite these similarities, there are some subtle differences in the two flow fields that might explain the increase in impingement tone amplitude with a 10 mm movement of the impingement plate. First of all, the structures in Figure 10, although present and organized, are not as well developed and not as large as the structures present in Figure 11. Rather, they seem to be more in a process of growth and development whereas the structures in Figure 11 are further along in the process. An attempt to elucidate this is made with the labeled structures in the figures. In Figure 10, the wavy region of fluid marked 'A' rolls up into a structure, grows and deforms as it interacts with the plate. In Figure 11, the structure marked 'B' in the 2nd frame undergoes a similar process of growth and interaction with the plate (or with the compression region set up in front of the plate). Unlike the development in Figure 10, however, this development leads to a larger and more coherent structure. Clearly, this analysis is inherently subjective, but there is an objective result that supports this analysis. The average flow images in Figure 7 clearly show a thicker mixing layer for ℓ=115 mm than for ℓ=105 mm. The thicker mixing layer is a direct result of faster growth and development of structures observed in the images of Figures 10 and 11.

The strong coupling between the nature of turbulence structures and the position of the impingement plate makes the impinging rectangular jet an ideal flow field for the investigation of aero-optics. The next step of this research is to incorporate a real-time Shack-Hartmann wavefront sensor to measure the degradation of an optical wavefront as it passes through a turbulent flow field. By simply adjusting the plate's location, many types of turbulent flow can be achieved. At one extreme (ℓ = 356 mm) there is a wide spectrum of scales of turbulence structures superimposed on a moderately organized asymmetric pattern of large-scale structures. At the other extreme (ℓ = 70 mm) the entire flow field is well organized and dominated by the growth and presence of large-scale structures with minimal presence of other scales of turbulence structures. The various flow fields available will allow us to study the degradation of an optical wavefront that occurs for a wide variety of turbulence scales and thus allow us to discriminate the effects of different scales.

Conclusions

The preliminary acoustic and flow visualization results presented here provide further insight into the coupling between large-scale coherent structures in the jet mixing layer and the impingement tones in the acoustic far field. The acoustic data were very rich in frequency content and exhibit various tonal features. Generally, the most dominant tones were observed for Strouhal numbers between 0.2 and 0.25. Four cases at ℓ = 70, 105, 115 and 356 mm with various tonal contents were chosen to represent typical features of the acoustic far field. The spectrum of ℓ = 356 mm was the baseline case and exhibited screech tones, but no impingement tones. In contrast, ℓ = 70 mm exhibited a condition of high resonance with many harmonics. The ℓ = 105 mm case did not exhibit any high amplitude (>110 dB) tones, while ℓ = 115 mm case had a single tone over 125 dB.

Flow visualizations were taken using the MHz rate imaging system at the same locations of ℓ = 70, 105, 115 and 356 mm. The visualizations showed varying degrees of organization of large-scale structures with the most organized flow occurring for the highly resonant case of ℓ = 70 mm. The flow was still moderately organized in an asymmetric pattern for the baseline case of ℓ = 356 mm, but was also marked by the presence of a wide spectrum of turbulence scales not present in the ℓ = 70 mm case. Not unexpectedly, large-scale structures form and interact with the impingement plate at the same frequencies observed in the acoustic far field. Also, larger and more coherent structures result in higher amplitude tones. This was explored by comparing the flow fields of ℓ = 105 and 115 mm where the ℓ = 115 mm flow field had slightly more developed structures that lead to the increase of impingement tone amplitude. This description of the flow field proved to be ideal for the next step of this research, which will incorporate a real-time Shack-Hartmann wavefront sensor to measure the degradation of an optical wavefront as it passes through the flow field.

Acknowledgements

The authors would like to thank AFRL/DAGSI (with Dr. Scott Harris) for supporting this research. The first author would like to thank the Department of Defense for his National Defense Science and Engineering Graduate fellowship.

References

Alvi, F. S., Ladd, J. A. and Bower, W. W., "Experimental and Computational Investigation of Supersonic Impinging Jets," AIAA J., Vol. 40, pp. 599-609, 2002.

Chew, L. and Christiansen, W., "Experimental Investigation of Transitional Free Shear Layer Optics," AIAA J., Vol. 31, pp. 2290-2295, 1993.

Elliott, G. S., Samimy, M., and Arnette, S. A., "A Study of Compressible Mixing Layers Using Filtered Rayleigh Scattering," AIAA Paper 92-0175.

Fitzgerald, E. J., and Jumper, E. J., "Aperture Effects on the Aerooptical Distortions Produced by a Compressible Shear Layer," AIAA J., Vol. 40, pp 267-275, 2002.

Hileman, J. and Samimy, M., "Turbulence Structures and the Acoustic Far Field of a Mach 1.3 Jet," AIAA Journal, Vol. 39, pp. 1716-1727, 2001.

Ho, C. M. and Nosseir, N. S., "Dynamics of an impinging jet. Part 1. The feedback phenomenon," J. Fluid Mech, Vol. 105. pp. 119-142, 1981.

Jumper, E. J., and Hugo, R. J., "Quantification of Aero-Optical Phase Distortion Using the Small-Aperture Beam Technique," AIAA J., Vol. 33, pp. 2151 – 2157, 1995.

Kerechanin, C., Samimy, M. and Kim, J.-H., "Effects of Nozzle Trailing Edge Modifications on the far-field acoustic Radiation in Supersonic Jets," AIAA Journal, Vol. 39, No. 6, pp. 1065-1070, 2001.

Krothapalli, A., "Discrete Tones Generated by an Impinging Underexpanded Rectangular Jet," AIAA J., Vol. 23, pp 1910-1915, 1985.

Krothapalli, A., Rajkuperan, E., Alvi, F. and Lourenco, L., "Flow field and noise characteristics of a supersonic impinging jet," J. Fluid Mech., Vol. 392, pp. 155-181, 1999.

Lempert, W. R., Wu, P. F., Zhang, B., Miles, R. B., Lowrance, J. L., Mastocola, V. J., and Kosonocky, W. F., "Pulse Burst Laser System for High-Speed Flow Diagnostics," AIAA Paper 96-0179.

Lempert, W. R., Wu, P. F., and Miles, R. B., "Filtered Rayleigh Scattering Measurements Using a MHz Rate Pulse-Burst Laser System," AIAA Paper 97-0500.

Raman, G. and Rice, E. J., "Mixing and Noise Benefit Versus Thrust Penalty in Supersonic Jets Using Impingement Tones," AIAA Paper 94-2955.

Raman, G., "Screech tones from rectangular jets with spanwise oblique shock-cell structures," J. Fluid Mech. Vol. 330 pp. 141-168, 1997

Rockwell, D. and Naudascher, E., "Self-Sustained Oscillations of Impinging Free Shear Layers," Ann. Rev. Fluid Mech., Vol. 11, pp. 67-94, 1979.

Tam, C. K. W. and Ahuja, K. K., "Theoretical Model of Discrete Tone Generation by Impinging Jets," J. Fluid Mech., Vol. 214, pp. 67-87, 1990.

Tam, C. K. W. and Norum, T. D., "Impingement Tones of Large Aspect Ratio Supersonic Rectangular Jets," AIAA J., Vol. 30, 1992.

Thurow, B., Hileman, J., Samimy, M., Lempert, W., "An In-Depth Investigation of Large Scale Structures in a Mach 1.3 Axisymmetric Jet," AIAA Paper 2001-0148.

Thurow, B., Hileman, J., Samimy, M. and Lempert, W., "Compressibility Effects on the Growth and Development of Large-Scale Structures in an Axisymmetric Jet," AIAA Paper 2002-1062, 2002.

Truman, C. R. and Lee, M. J., "Effects of organized turbulence structures on the phase distortion in a coherent optical beam propagating through a turbulent shear flow," Physics of Fluids A, Vol. 2, pp. 851-857, 1990.

Wu, P., Lempert, W. R. and Miles, R. B., "MHz Pulse Burst Laser System and Visualization of Shock-Wave/Boundary Layer Interaction in a Mach 2.5 Wind Tunnel," *AIAA J.*, Vol. 38, pp.672- 2000

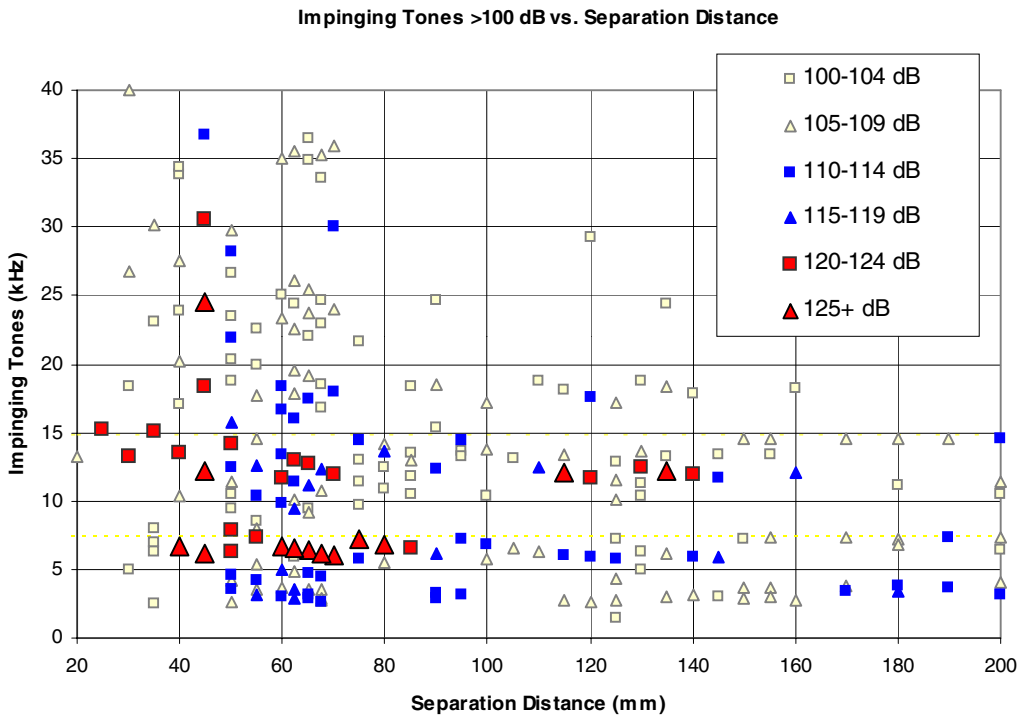

Figure 1 – All impingement tones with magnitude larger than 100 dB.

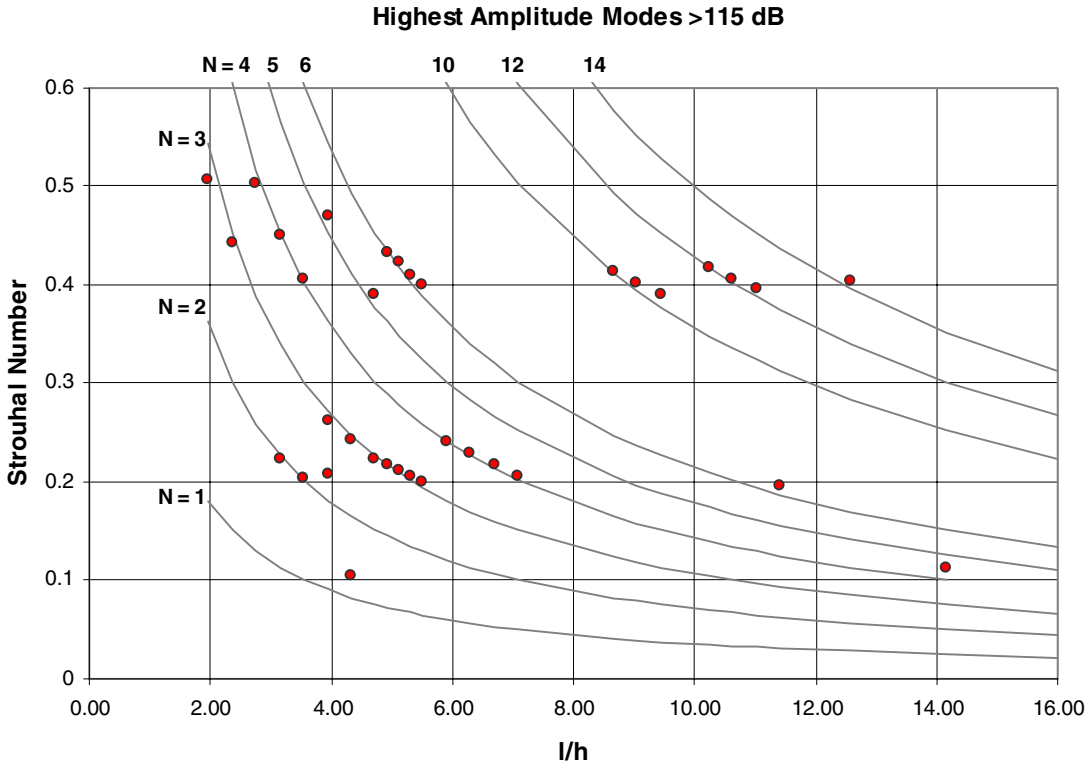

Figure 2 – Non-dimensional impingement tones with magnitude larger than115 dB. Lines drawn through data are theoretical values of impingement tones with mode number marked.

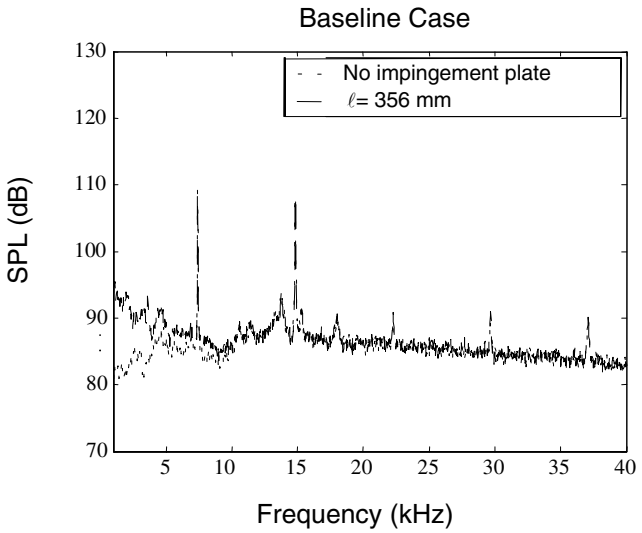

Figure 3 – Spectra of impinging jet baseline cases (ℓ/h = 28 & inf).

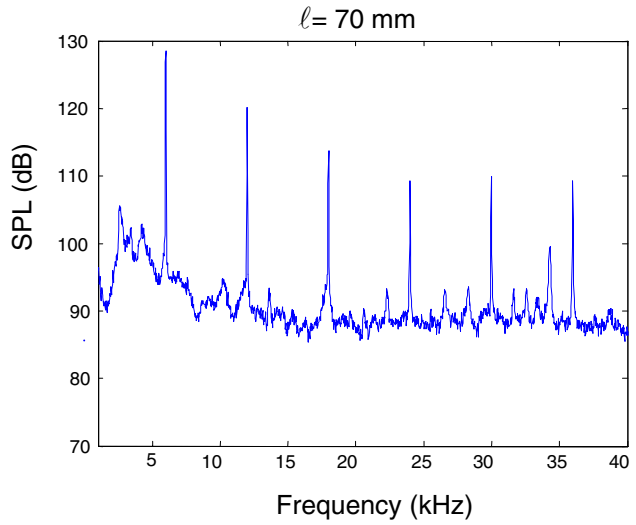

Figure 4 – Spectrum of impinging jet with ℓ= 70 mm (ℓ/h = 5.5).

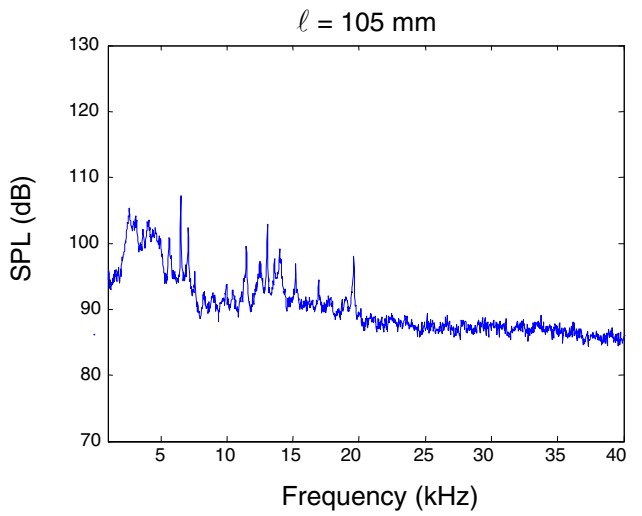

Figure 5 – Spectrum of impinging jet with ℓ = 105 mm (ℓ/h = 8.3).

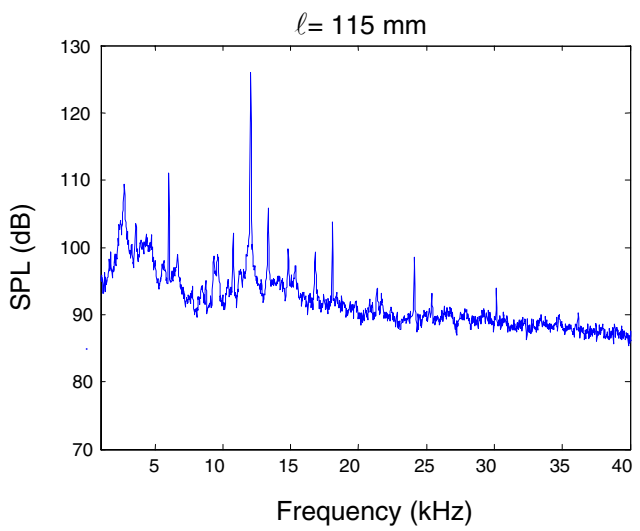

Figure 6 – Spectrum of impinging jet with ℓ = 115 mm (ℓ/h = 9.1).

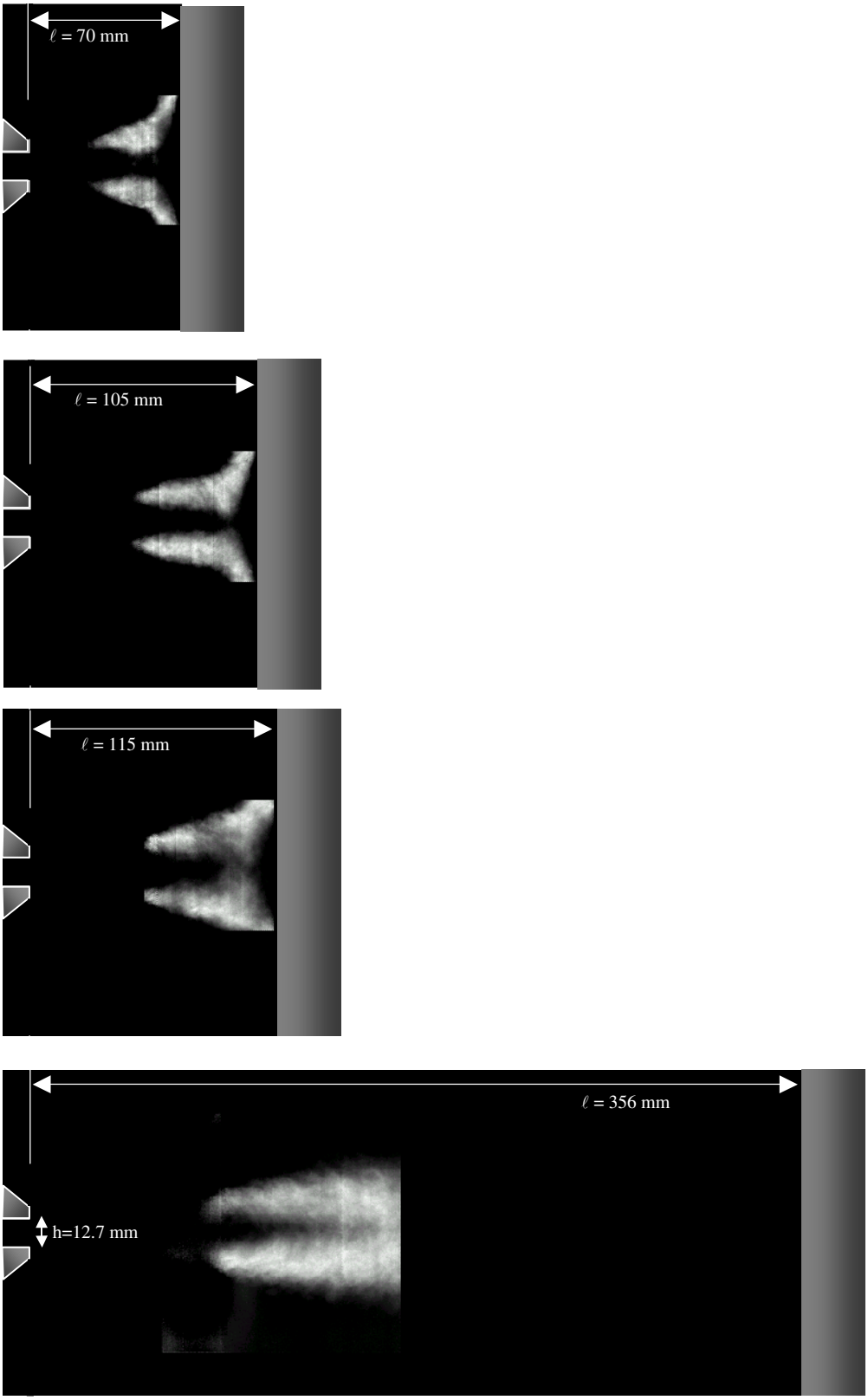

Figure 7 – Average flow visualization images of impinging jet at plate separation distances of 70, 105, 115, and 356 mm.

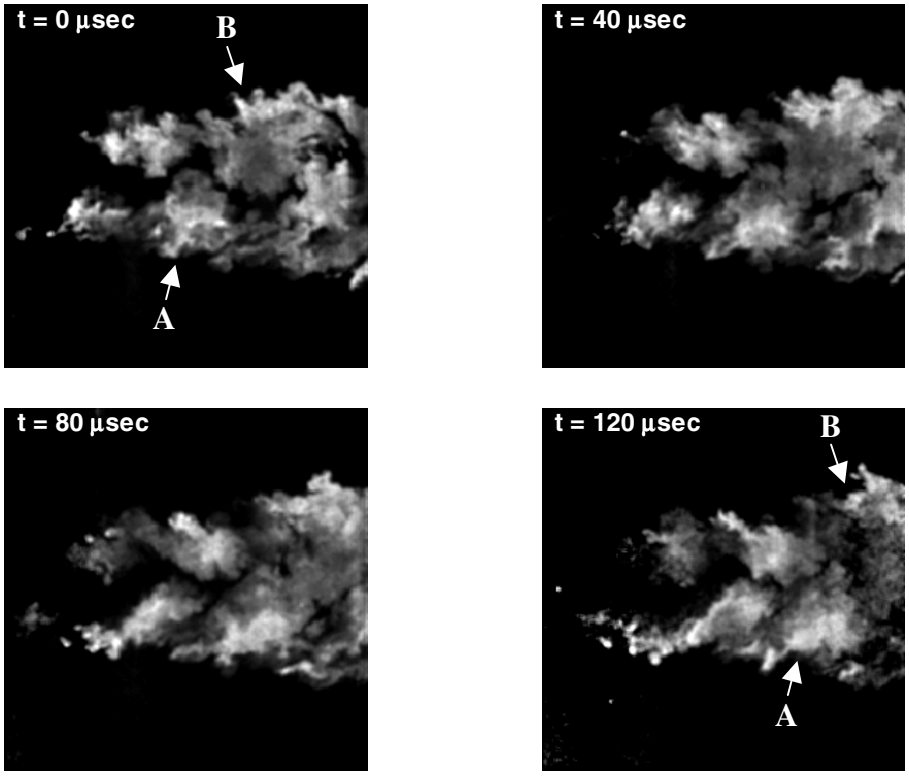

Figure 8 – Instantaneous images of the impinging jet with separation distance of 356 mm (ℓ/h = 28)

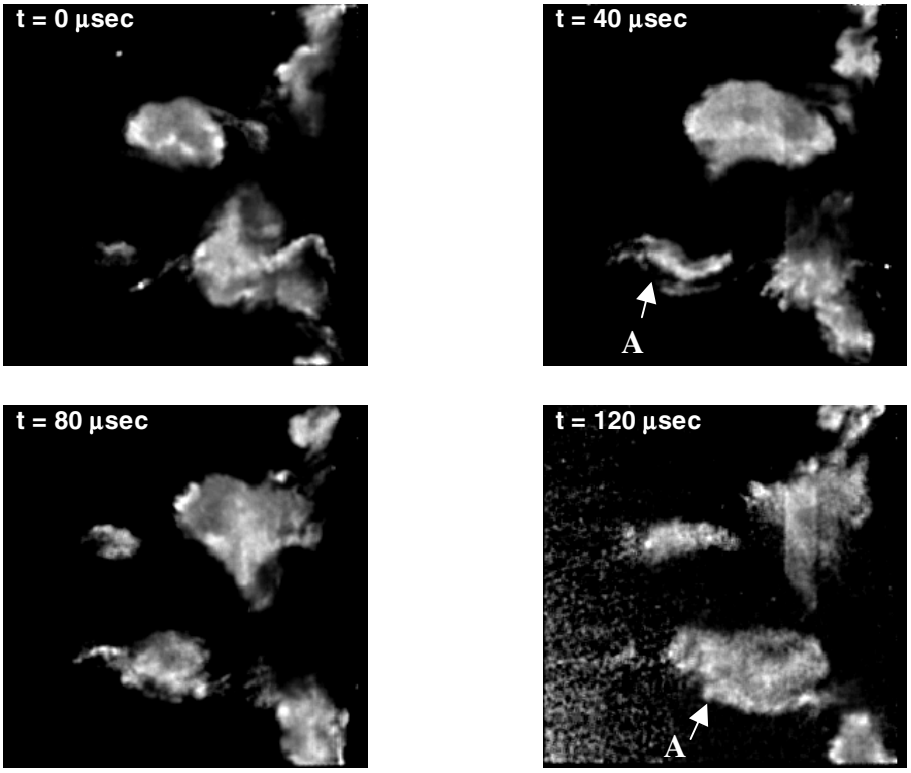

Figure 9 – Instantaneous images of impinging jet with separation distance of 70 mm (ℓ/h = 5.5).

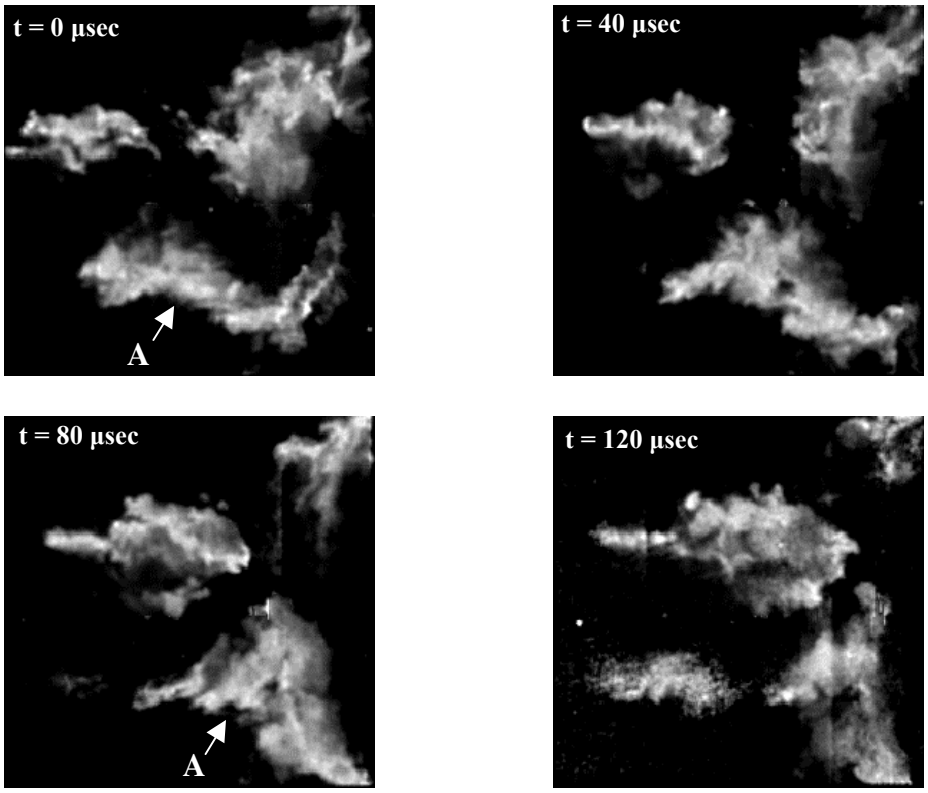

Figure 10 – Instantaneous images of impinging jet with separation distance of 105 mm (ℓ/h = 8.3).

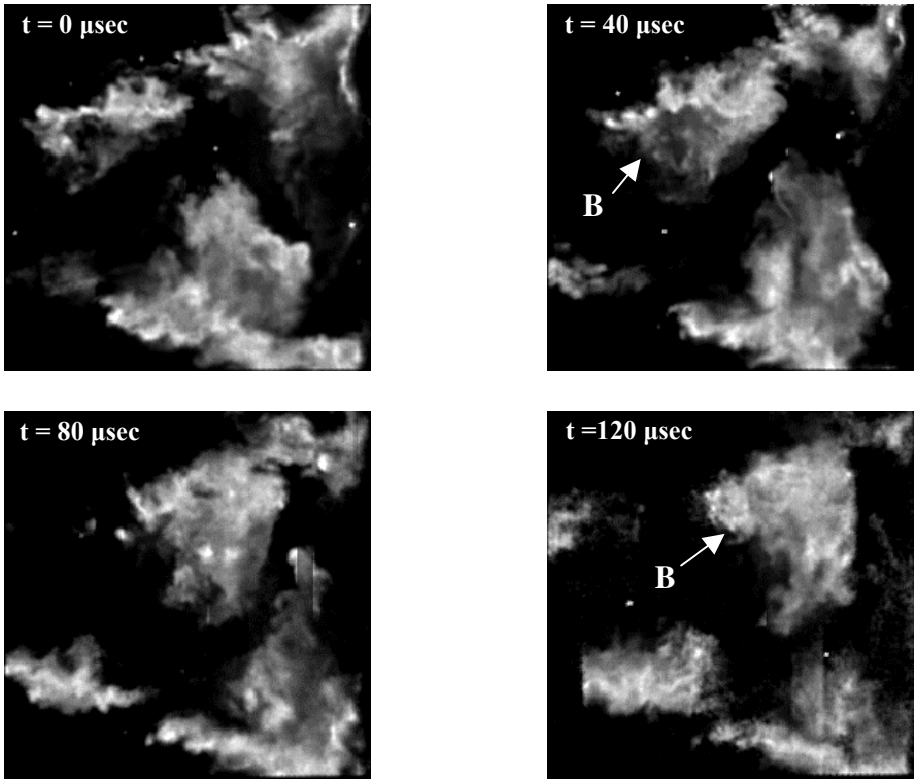

Figure 11 – Instantaneous images of impinging jet with separation distance of 115 mm (ℓ/h = 9.1).